NJC

Accepted Manuscript

This article can be cited before page numbers have been issued, to do this please use: N. A and V. Alexander, *New J. Chem.*, 2016, DOI: 10.1039/C5NJ03393D.

View Article Online
DOI: 10.1039/C5NJ03393D

NJC

ARTICLE

A tri- (Ru^{II}-Gd_2^{III}) and tetranuclear (Ru^{II}-Gd_3^{III}) *d-f* Heterometallic Complexes as Potential Bimodal Imaging Probes for MRI and Optical Imaging

A. Nithyakumar and V. Alexander*

Synthesis of a tri- and a tetranuclear Ru^{II}-Gd_2^{III} and Ru^{II}-Gd_3^{III} *d-f* heterometallic complexes of 4-aminopyridine appended DO3A (DOTA-AMpy, **4**) with 1,10-phenanthroline and 4′-(*p*-tolyl)-2,2′:6′,2″-terpyridine ancillary ligands and their relaxometry and in vitro cytotoxicity studies are reported. The complexes $[Ru(phen)_2\{Gd(DOTA\text{-}AMpy)(H_2O)\}_2]Cl_2$ (**7**) and $[Ru(ttpy)\{Gd(DOTA\text{-}AMpy)(H_2O)\}_3]Cl_2$ (**9**) exhibit the "per Gd" longitudinal relaxivity of 6.19 and 7.47 $mM^{-1}s^{-1}$ and 15.37 and 18.61 $mM^{-1}s^{-1}$, respectively, in aqueous solution and in the presence of HSA (20 MHz, pH = 7.4, Phosphate buffer saline, 37 °C). The complex **7** exhibits an emission band at 590 nm. The cell viability and cytotoxicity study of the complexes **7** and **9** against the HeLa cell lines, studied by MTT assay, demonstrates their cytotoxic activity with the IC_{50} values of 52.1 and 27.9 μM, respectively. Morphological assessment of apoptosis by acridine orange and ethidium bromide staining and by Hoechst-33342 assay show marked morphologic signs of apoptosis in a dose-dependent manner. Flow cytometric analysis by propidium iodide staining indicates inhibition of HeLa cell proliferation and DNA ladder assay show apoptotic cell death lending support for the antitumor activity of **7** and **9**. Molecular docking study reveals that the complexes intercalate with DNA and bind with HSA. The relaxometry and and cytotoxicity studies indicate that the complexes **7** and **9** could be used as potential bimodal imaging probes and as anticancer agents.

Received 00th 2015,
Accepted 00th 2015

DOI: 10.1039/x0xx00000x

www.rsc.org/

Introduction

Gadolinium(III) complexes are widely utilized as contrast agents (CAs) for magnetic resonance imaging (MRI) in clinical diagnosis.[1] Among the multiple diagnostic imaging techniques, MRI is especially advantageous as a noninvasive modality: it can image deep into tissues, there is no ionizing radiation, it provides 3D images with submillimeter spatial resolution, excellent soft tissue contrast, there are multiple types of contrast available, the imaging is not operator dependent, and it can provide whole body images with excellent spatial and anatomical resolution.[1,2] Ever since the introduction of MRI as a diagnostic tool, the interest in the development of efficient, responsive, and tissue-specific CAs has grown tremendously.[3] Despite the high spatial resolution and tissue penetration of MRI, this technique suffers from a low sensitivity. Further, the efficiency of commercial MRI contrast agents is too low for the application of MRI to molecular imaging.

Luminescence-based imaging, on the other hand, can provide high resolution images, but this technique is only suitable for thin tissue samples because of the low optical transparency of biological tissues.[4] As the optical imaging technique is much more sensitive than MRI, the combination of these two techniques may result in images which reveal more details than when the two techniques are used separately. In the search for the development of new, promising contrast agents, multimodal imaging agents are gaining nowadays great attention in the field of clinical and preclinical imaging applications to investigate samples in exquisite detail.[5] Thus, bimodal optical/MRI reporters are of high interest because they combine the high resolution of MRI with the high sensitivity of optical imaging.[6] The possibility of using bimodal imaging probes which permit simultaneous microscopy and whole body imaging is explored and the recent developments in the field of combined MRI/optical probes is reviewed.[7] The relatively long lived luminescence from lanthanide and transition metal complexes makes them ideal as probes for time-gated luminescence based assay and imaging.[8]

The use of Gd(III)-containing *metallostars* as MRI CAs is gaining attention because of their improved relaxometric properties.[9] Furthermore, it has been shown that heteropolymetallic complexes combining gadolinium and luminescent transition metal ions can potentially be used as CAs for bimodal imaging.[10] Ru(II) polypyridine complexes display emission in the visible region with lifetimes in the microsecond range that allows their use in time-resolved applications, large Stokes shift (> 5000 cm^{-1}) that minimizes self-quenching, and high photostability that permits continuous monitoring of biological

Department of Chemistry, Loyola College, Chennai 600034, India.
E-mail: valexander@rediffmail.com; Fax: +91-44-28175351; Tel: +91-44-28175351
† Electronic Supplementary Information (ESI) available: See DOI: 10.1039/x0xx00000x

View Article Online
DOI: 10.1039/C5NJ03393D

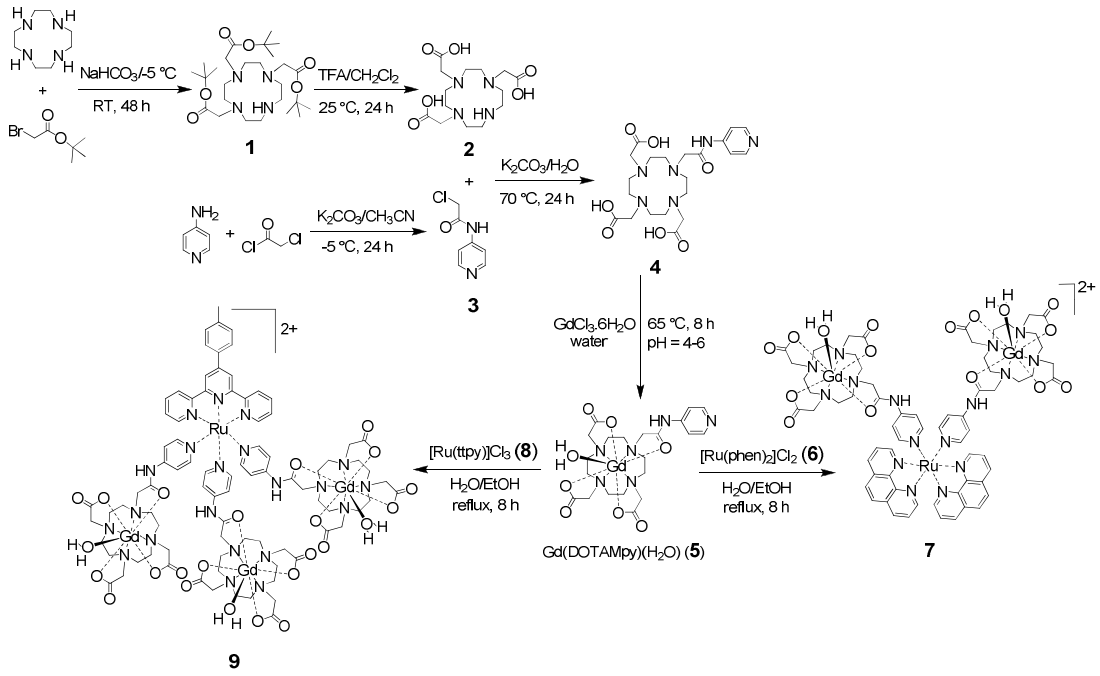

Scheme 1. Synthesis of the ligand DOTA-AMpy (**4**) and the Ru^{II}-Gd^{III} tri- and tetranuclear heterometallic complexes.

events by fluorescence spectroscopy and microscopy.[11] Thus, Ru-Gd *d-f* heterometallic assemblies have the potential to function as bimodal imaging probes combining the good spatial resolution of the MRI technique with the high resolution images of thin tissue samples or cells with luminescence based imaging,[4,10a] leading to complementary information.[6b,10a] Other *d-f* heterometallic bimodal imaging probes reported are: Ru-Gd_6 metallostar by Bunzli et al.,[12] Ru-Gd heterobimetallic complex by Parac-Vogt et al.,[13] Re-Gd single molecule dual imaging agent by Faulkner et al.,[10a] heterobimetallic Ru-Gd_3 metallostars by Parac-Vogt et al.,[14] and by Picard et al.,[15] and a tripodal Ru-Gd_3 metallostar by De Borggraeve et al.,[16] Heterometallic *f-f* assemblies such as Eu-Gd dinuclear complex[17] and Eu-Gd_3 heteropolymetallic complex[18] containing both Gd and luminescent lanthanide metal ions are also reported as bimodal imaging probes.

Ru(II) polypyridyl complexes are used as potent anticancer agents,[19] DNA probes,[20] DNA intercalators,[21] in cellular imaging,[22] and in protein monitoring.[23] Although multimodal imaging agents are developing at a growing pace, a challenge that needs to be overcome in the development of *d-f* heterometallic systems suitable for medical applications is achieving good solubility in water. We have recently reported a Ru^{II}-Gd^{III}_2 *d-f* heterometallic assembly as a potential bimodal imaging probe for MR and fluorescence imaging.[24] In this paper we report the synthesis, photophysical, relaxometric, and in vitro fluorescence imaging study of a trinuclear Ru^{II}-Gd^{III}_2 and a tetranuclear Ru^{II}-Gd^{III}_3 *d-f* heterometallic complexes incorporating the Gd(III) chelates of 4-aminopyridine-appended DO3A (Scheme 1) as bimodal MRI/optical imaging probes and their cytotoxicity towards the HeLa cell lines.

Results and discussion

Synthesis of ligand and characterization. 4′-(*p*-Tolyl)-2,2′:6′,2″-terpyridine (ttpy) is synthesized by the one pot synthetic protocol[25] based on Hantzsch synthesis (pyridine ring fusion). The pyridine-amide linker molecule **3** is synthesized by the reaction of 4-aminopyridine with chloroacetyl chloride in dry acetonitrile at -5 °C in the presence of potassium carbonate as the proton scavenger. The pyridine-amide linker appended DO3A (DOTA-AMpy, **4**) is synthesized by the reaction of DO3A with **3** in a 1:1 mole ratio in water in the presence of potassium carbonate at 70 °C for 24 h.

Synthesis of complexes and characterization. *cis*-$[Ru(phen)_2Cl_2]$[26] (**6**) and $[Ru(ttpy)Cl_3]$[27] (**8**) are synthesized by the literature procedure. The gadolinium(III) complex $[Gd(DOTA\text{-}AMpy)(H_2O)]$ (**5**) is synthesized by the reaction of gadolinium(III) chloride hydrate with the preformed ligand DOTA-AMpy (**4**) in a 1:1 mole ratio in water at 70 °C for 24 h. The ESI-MS of **5** shows peaks at *m/z* 633 and 679 corresponding to the species $[M\text{-}H]^+$ and $[M\text{-}H+2Na]^+$, respectively (Fig. S12 in the ESI). The heterometallic trinuclear complex $[Ru(phen)_2\{Gd(DOTA\text{-}AMpy)(H_2O)\}_2]Cl_2$ (**7**) is synthesized by the reaction of *cis*-$[Ru(phen)_2Cl_2]$ (**6**) with **5** in a 1:2 mole ratio in water/ethanol (1:1, v/v) under reflux in an argon atmosphere for 8 h (Scheme 1) followed by purification by preparative reversed-phase high-performance liquid chromatography. The complex is isolated as a dark yellow solid and its purity is checked by analytical HPLC (Fig. S13 in the ESI). The ESI-MS of the complex **7** shows peaks at *m/z* 556 and 615 corresponding to the species $[M\text{-}2Cl\text{-}H_2O+6H]^{3+}$ and $[M\text{-}H+4Na]^{3+}$, respectively (Fig. S14 in the ESI). The heterometallic tetranuclear complex [Ru(ttpy){Gd(DOTA-AMpy)-

View Article Online
DOI: 10.1039/C5NJ03393D

$(H_2O)\}_3]Cl_2$ (**9**) is synthesized by reaction of $[Ru(ttpy)Cl_3]$ (**8**) with **5** in a 1:3 mole ratio in water/ethanol (1:1, v/v) in the presence of *N*-methylmorpholine under reflux in an argon atmosphere (Scheme 1) followed by purification by preparative reversed-phase high-performance liquid chromatography. The complex is isolated as a red solid and its purity is checked by analytical HPLC (Fig. S15 in the ESI). The ESI-MS of the complex **9** shows peaks at *m/z* 1209 and 374 corresponding to the species $[M\text{-}2Cl\text{-}H_2O\text{+}3H\text{+}3Na]^{2+}$ and $[M\text{-}2Cl\text{-}5H_2O\text{+}H]^{6+}$, respectively (Fig. S16 in the ESI). When the complex $[Gd(DOTA\text{-}AMpy)(H_2O)]$ (**5**) is reacted with the preformed Ru(II) complexes, the pyridine pendant arm of the Gd-bound DOTA-AMpy ligand coordinates with the Ru(II) metal ion and forms the heterometallic Ru^{II}-Gd^{III} complexes by self-assembly with phen or ttpy ancillary ligands.

Photophysical studies. Photophysical studies. The electronic absorption spectra of the complexes $[Ru(phen)_2\{Gd(DOTA\text{-}AMpy)(H_2O)\}_2]Cl_2$ (**7**) and $[Ru(ttpy)\{Gd(DOTA\text{-}AMpy)(H_2O)\}_3]Cl_2$ (**9**) in 0.1 M Tris-HCl buffer at 298 K contain an absorption band at 473 and 493 nm due to the spin-allowed ^{1}MLCT transition and an absorption band at 265 and 273 nm assignable to the ligand-centered π→π* transition, respectively (Fig. S17 in the ESI). The excitation spectrum of the complex **7** contains an excitation maxima at 447 nm. Upon excitation it exhibits an emission band at 590 nm, characteristics of the Ru(II) polypyridine complex originating from the ^{3}MLCT excited state, at room temperature (298 K). At 77 K, the emission maxima is slightly blue-shifted to 586 nm. The complex **9** does not emit at room temperature due to the thermal quenching of the lowest lying ^{3}MLCT (Ru-tpy) excited state by the nonradiative decay of the low-lying ^{3}MC state. At 77 K, it exhibits an emission band at 644 nm. The photophysical properties of the complexes are comparable to that of other luminescent Ru(II) polypyridine complexes.[10a,16,28] In these Ru^{II}-Gd^{III} heterometallic complexes the Ru(II) luminescence is not quenched by the Gd(III) ion since its excited states energies are much higher (> 31,000 cm^{-1}) than that of the ^{3}MLCT state of Ru(II) chromophore, preventing any Ru→Gd energy transfer process.[15] The normalized emission spectra of the complexes in 0.1 M Tris-HCl buffer are presented in Fig. 1.

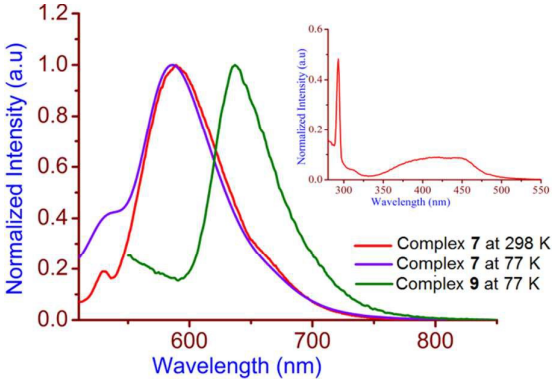

Fig. 1 Normalized emission spectra of the complexes **7** and **9** in 0.1 M Tris-HCl buffer (pH = 7.4) at 25 °C. Inset: excitation spectra (λ_{ex} = 447 and 454 nm).

Relaxometric studies. The efficiency of an MRI contrast agent is usually measured by its water proton relaxivity (r_{1p}), defined as the paramagnetic longitudinal relaxation rates induced by a 1 mM solution of the contrast agent. The complexes **7** and **9** exhibit the "per Gd" longitudinal relaxivity of 6.19 and 7.47 $mM^{-1}s^{-1}$ (pH = 7.4, PBS, 20 MHz, and 37 °C), respectively, which is significantly higher than that of $[Gd(DOTA)(H_2O)]^-$ (3.38 mM^{-1} s^{-1}, 37 °C)[29] and $[Gd(DO3A)(H_2O)_2]$ (4.80 mM^{-1} s^{-1}, 40 °C).[30] The DOTA-amide derivative DOTA-AMpy (**4**) coordinates with the Gd(III) ion through the four ring nitrogen, three carboxylate oxygen, and the amide oxygen donors with one coordinated water molecule (q = 1).[17,31] The higher "per Gd" longitudinal relaxivity of the complexes **7** and **9** compared to that of $[Gd(DOTA)(H_2O)]^-$ and $[Gd(DO3A)(H_2O)_2]$ is attributed to an increase in their molecular weight. As the molecular weight and dimension of a complex increases its molecular tumbling rate decreases leading to high proton relaxivity. However, the "per Gd" relaxivity of **7** and **9** are lower than that of the other heterometallic assemblies such as $[Fe\{Gd_2bpy(DTTA)_2(H_2O)_4\}_3]^{4-}$ (r_{1p} = 9 $mM^{-1}s^{-1}$),[9b] $[\{Gd(DTPA\text{-}ph\text{-}phen)\}_3(H_2O)_3Ru]^-$ (r_{1p} = 12 $mM^{-1}s^{-1}$),[14] $[Ru\{Gd_2bpy(DTTA)_2(H_2O)_4\}_3]^{4-}$ (r_{1p} = 12.5 $mM^{-1}s^{-1}$),[12] and $[Ru(Gd\text{-}PMNTA)_3(H_2O)_6]^-$ (r_{1p} = 17.0 $mM^{-1}s^{-1}$).[15]

Interaction of the Complexes with HSA. The "per Gd" longitudinal proton relaxivity of the complexes **7** and **9** in PBS containing 4.5% HSA are 15.37 and 18.61 mM^{-1} s^{-1}, respectively, which is about 3.0 and 2.5 times higher than their relaxivities in the absence of HSA. The increase in the longitudinal relaxivity of the complexes in the presence of HSA confirms their binding with the HSA.

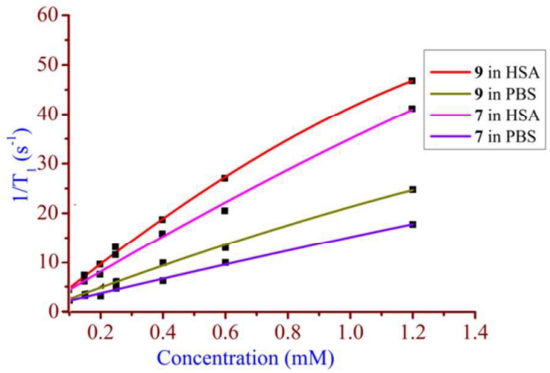

Fig 2. Plot of the concentration of the complexes **7** and **9** versus $1/T_1$ in PBS and in the presence of HSA (pH = 7.4, 37 °C).

The interaction between the complexes and HSA is confirmed by ultrafiltration method and the estimated association constants are K_a = 6980 ± 748 and 7379 ± 658 M^{-1}, respectively, obtained by fitting the data in eq 1.[13] The number of equivalent and independent sites is set to be 1.

$$R_1^{p,obs} = 1000\{(r_1^f s^0) + 0.5(r_1^c - r_1^f)[Np^0 + s^0 + K_a^{-1}] - \sqrt{[(Np^0 + s^0 + K_a^{-1})^2 - 4Ns^0p^0]}\} \quad (1)$$

where, p^0 is the protein concentration, s^0 is the concentration of the paramagnetic complex, r_1^f is the relaxivity of the free complex, r_1^c is the relaxivity of the noncovalently bound complex, and N is the number of independent and identical interaction sites. A decrease

View Article Online
DOI: 10.1039/C5NJ03393D

in the mobility of the adduct formed by the complexes with HSA leads to an increase in their proton relaxation rates. The plot of the concentration of the complexes **7** and **9** versus $1/T_1$ in PBS and in the presence of HSA are depicted in Fig. 2.

Cell viability and cytotoxicity study by MTT assay. The MTT (MTT = 3-(4,5-dimethylthiazol-2-yl)-2,5-diphenyltetrazolium bromide) assay is a rapid quantitative colorimetric assay developed by Mosmann[32] for mammalian cell survival and proliferation. It is based on the ability of live cells to convert the pale yellow MTT into a dark blue formazan product by the cleavage of the tetrazolium ring in active mitochondria. This method detects living, but not dead cells and the absorbance of the color generated (optical density) is dependent on the degree of activation of the cells and can, therefore, be used to measure cytotoxicity, proliferation, or activation.[33] The MTT assay is performed to evaluate the cytotoxic effects of the Ru^{II}-Gd^{III} complexes against the HeLa cell lines. The HeLa cell lines treated with 1 and 10 μM solution of the complexes for 48 h at 37 °C in PBS display moderate cytotoxic activity, whereas at 25 μM concentration of the complexes the cell viability is 49.2 and 38.6%, respectively. When the HeLa cell lines are treated with 50 μM solution of the complexes the cell viability is 19.5 and 16.5%, respectively (Fig. S18 in the ESI). The IC_{50} values of the complexes **7** and **9** are 52.1 and 27.9 μM, respectively. These results indicate that the complexes exhibit good cytotoxic activity against the HeLa cell lines and have the potential to be explored as anticancer agents.

Cell viability assay by Hoechst-33342 staining. Hoechst stains are a family of blue fluorescent dyes used to stain DNA,[34] developed by Hoechst AG. This protocol describes the use of Hoechst 33342 (2'-(4-ethoxyphenyl)-5-(4-methyl-1-piperazinyl)-2,5'-bi-1H-benzimidazole trihydrochloride trihydrate) to label nuclear DNA of cells grown in cultures. It is a cell permeable fluorescent compound and, thus, stains live cells by binding with high affinity to the adenine-thymine (A-T) rich region of DNA in the minor groove. On binding with DNA it emits blue fluorescent emission upon excitation in the UV region. The HeLa cell lines are incubated with the complexes **7** and **9** at two different concentrations (25 and 50 μM) for 24 h at 37 °C and stained with Hoechst-33342 and examined by fluorescent microscopy.

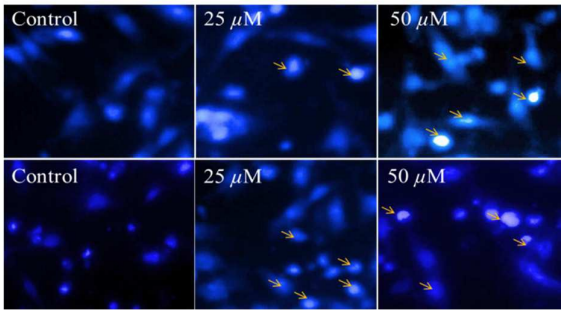

Fig 3. Morphological changes observed for the HeLa cell lines incubated with the complexes **7** (top row) and **9** (bottom row) for 24 h, 37 °C at 25 and 50 μM concentrations and stained with Hoechst-33342.

The HeLa cell lines incubated with 25 μM solution of the complexes display a weak fluorescence with significant cell reduction, whereas at 50 μM concentration of the complexes the cells display the fluorescence of the apoptotic cells with marked morphological signs of apoptosis such as cell reduction, cell shrinkage, rounding of the cells, increase in the detached cells, decrease in the adherent cells, and the appearance of a large number of suspended cells accompanied by cell debris, apoptotic bodies, and other characteristics. While apoptotic bodies displaying different size and irregular morphology are observed upon incubation of the HeLa cell lines with the complexes, no such changes are observed in the control group. Fig. 3 clearly indicates that the density of the cells gradually decreases while increasing the concentration of the complexes. These results indicate that the complexes **7** and **9** induce apoptosis in a dose-dependent manner on the HeLa cell lines and demonstrates the utility of the complexes as potential anticancer agents.

Morphological assessment of apoptosis by acridine orange (AO) and ethidium bromide (EB) dual staining. When cells are exposed to cytotoxic agents, there are various patterns of cell death that they may undergo. The two major types of cell death are apoptosis and necrosis. Apoptosis or programmed cell death can be initiated by two central mechanisms, the extrinsic (death receptor) and intrinsic (mitochondrial) pathways. Apoptosis is characterized by cell shrinkage, chromatin condensation, and blebbing of the plasma membrane.[35] The HeLa cell lines incubated with 25 μM solution of the complexes **7** and **9** for 24 h at 37 °C and stained with AO and EB display the green fluorescence of early apoptotic cells and weak red fluorescence of necrotic cells with condensed structure. When the cell lines are incubated with 50 μM solution of the complexes they display the bright green fluorescence (blue arrow) of apoptotic cells and the red fluorescence of necrotic cells (white arrows) with cell reduction and chromatin condensation as shown in Fig. 4. As the concentration of the complexes increases there is an increase in the appearance of the apoptotic nuclear bodies in the HeLa cell lines, wherein the nuclei have been condensed. The results indicate that the complexes **7** and **9** exhibit the dose-dependent inhibition effect on the cancer cell lines, whereas the control HeLa cell lines do not show any change in their nuclear morphology.

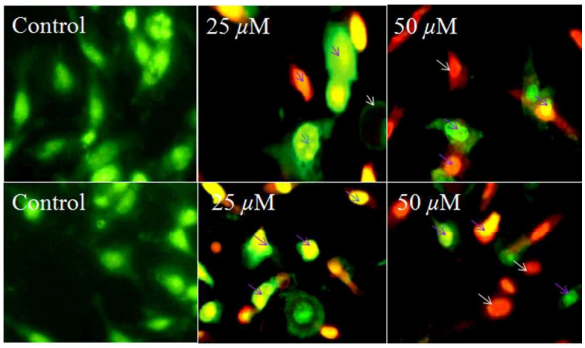

Fig 4. Fluorescence images of the HeLa cells incubated with the complexes **7** (top row) and **9** (bottom row) for 24 h, 37 °C at 25 and 50 μM concentrations and stained with acridine orange and ethidium bromide (AO/EB).

View Article Online
DOI: 10.1039/C5NJ03393D

Flow cytometric analysis of cell cycle by propidium iodide staining. Cell cycle analysis employs flow cytometry to distinguish cells in different phases of the cell cycle. The flow cytometric analysis of cell cycle by propidium iodide (PI) staining has been widely used for the rapid and quantitative evaluation of cell apoptosis.[36] Incubation of the HeLa cell lines with the complexes **7** and **9** followed by staining with PI reveals nuclear staining of the chromosomal DNA. Fig. 5 shows the cell cycle profile of the HeLa cell lines incubated with 25 μM solutions of the complexes for 24 h at 37 °C. Upon incubation of the HeLa cell lines with the complexes there is an increase in the proportion of the cells in the G_2/M phase from 18.89% for the control to 41.50% in the presence of the complex **7** and 82.33% in the presence of the complex **9**. Fig. 5 indicates that the complexes inhibit the HeLa cell proliferation by inducing the cell cycle arrest in the G_2/M phase and shows a dose-dependent inhibition effect on the cell proliferation.

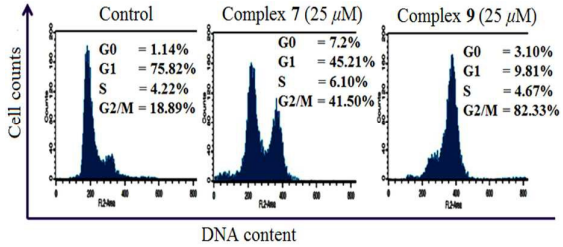

Fig 5. The cell cycle profiles of the HeLa cell lines incubated with 25 μM solutions of complexes **7** and **9** for 24 h, 37 °C and stained with propidium iodide after fixation.

Apoptotic DNA ladder assay. DNA laddering is a distinctive feature of DNA degraded by caspase-activated DNase (CAD), which is a key event during apoptosis. CAD cleaves genomic DNA at internucleosomal linker regions, resulting in DNA fragments that are multiples of 180-185 base-pairs in length. Separation of the fragments by agarose gel electrophoresis results in a characteristic "ladder" pattern.[37] The dose-dependent inhibition effects of the complexes **7** and **9** on the HeLa cell lines is confirmed by DNA fragmentation assay.

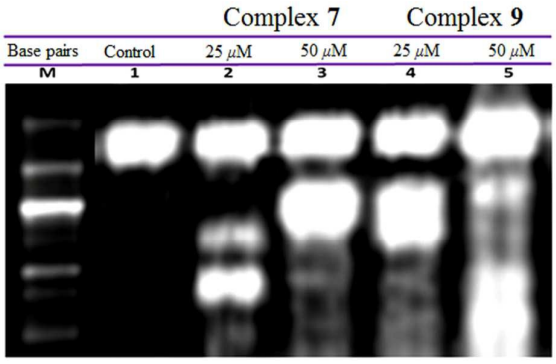

Fig 6. DNA ladder assay: HeLa cell lines incubated with the complexes **7** and **9** at 25 and 50 μM concentrations in DMEM medium.

The HeLa cells are incubated with different concentrations of the complexes (M, base pair; control, lane 1; 25 μM, lane 2; 50 μM, lane 3 for the complex **7**; 25 μM, lane 4 and 50 μM, lane 5 for the complex **9**) in DMEM culture medium at 37 ^{o}C for 24 h. The DNA fragments from both the samples are isolated, subjected to 1.2% agarose gel electrophoresis, and photographed in a gel documentation system. The images of both the test samples exhibit ladder formation as shown in Fig. 6, indicating cell apoptosis, whereas the DNA isolated from the control HeLa cell lines does not exhibit any ladder formation. The results indicate that the complexes promote apoptosis in the HeLa cell lines lending support for their antitumor activity.

DNA intercalation. Intercalation is defined as the non-covalent stacking interaction occurring due to the insertion of planar heterocyclic aromatic rings between base pairs of the DNA double helix.[38] To elucidate the mode of interaction and binding affinity, molecular docking studies have been performed on DNA (PDB ID: 1BNA) with the complexes **7** and **9**. The planarity of the 1,10-phenanthroline and tolylterpyridine ligands coordinated to the Ru(II) centre are compatible for strong π-π stacking interactions. Our docking results show that the complex **7** binds with the major groove with a better match inside the DNA strands which facilitates hydrogen bonding with the G-C and A-T rich region of the d(CGCGAATTCGCG) sequence, while the complex **9** intercalates with the DNA and does not form hydrogen bonding. The overall geometric shape and complementary score value of the complexes **7** and **9** are 4870 and 6250, respectively. Graphical representation of the intercalated complexes with the DNA is given in Fig. 7.

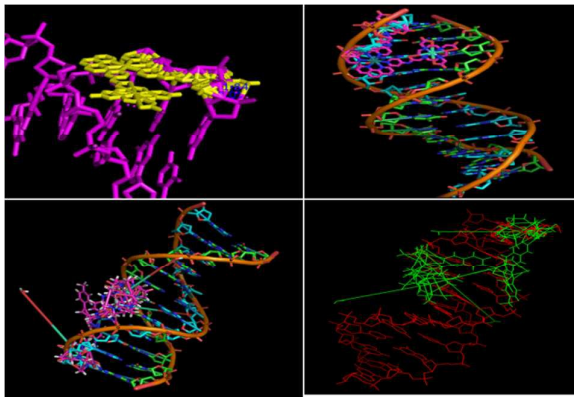

Fig 7. Graphical representation of the intercalated complexes **7** (top row) and **9** (bottom row) with DNA (PDB ID: 1BDNA).

Molecular docking with HSA. Human serum albumin (HSA) is the most abundant protein in the blood plasma which accounts for about 60% of the plasma's total protein contents. The molecular docking results reveal that the complexes **7** and **9** have good binding affinity towards the protein receptor with a binding energy of -466.84 and -476.85 kcal mol^{-1}, respectively. The amino acids involved in binding with the protein receptor are ALA 194, ARG 145, ARG 197, ASP 108, GLN 459, GLU 425, HIS 146, LYS 190, PHE 149, PRO 147, TRY 148, and SER 193. Structural studies have shown that HSA consists of three homologous domains: I (residues 1-195), II (196-383), and III (384-585). The complexes are bound to HSA by electrostatic and hydrogen bonding interactions. The distance of separation between the hydrogen bonded protons of the protein

View Article Online
DOI: 10.1039/C5NJ03393D

and the nitrogen and oxygen atoms of the bound complexes, computed using MM software HEX 5.0, are 3.12 and 3.47 Å for the complex **7** and 3.45, 2.96, and 3.51 Å for the complex **9**, indicating that the complex **7** is in close proximity to the THE 161 and PHE 134 amino acids, while the complex **9** is in close proximity to the SER 517, ARG 186, and HIS 146 amino acids. The possible hydrogen bonding interactions between the complexes with the receptor are presented in Fig. 8.

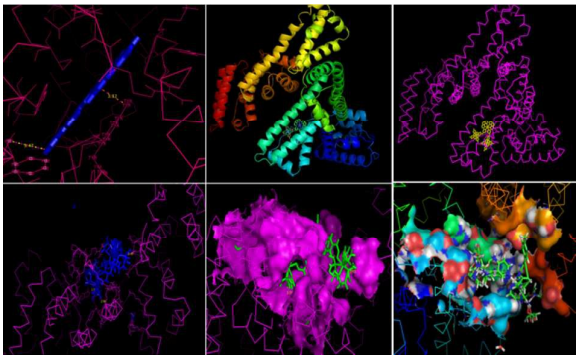

Fig 8. Molecular docked model of the complexes **7** (top row) and **9** (bottom row) with HSA (PDB ID: 1h9z).

Conclusions

The tri- and tetranuclear Ru^{II}-Gd_2^{III} and Ru^{II}-Gd_3^{III} *d-f* heterometallic complexes function as contrast enhancing agents for MRI and as optical probes for fluorescence imaging. Our study demonstrates that the complexes have good cell membrane permeability which promises their use for further in vitro and in vivo studies. In vitro cytotoxicity studies using cultured HeLa cell lines show that the complexes **7** and **9** exhibit good anticancer activity and the results may be useful in the development of new anticancer agents. The DOTA-AMpy type ligand framework is suitable for the development of a variety of *d-f* heterometallic assemblies by replacing the pyridine pendant arm by other polypyridine ligands. The fluorescence properties and the binding affinity of such complexes could be finetuned by changing the ancillary ligands coordinated to the Ru(II) center. The synthetic strategies developed in the present work could be exploited to develop a variety of *d-f* heterometallic assemblies.

Experimental

Materials. All reagents and solvents were of analytical reagent grade and used without further purification. 1,4,7,10-Tetraazacyclododecane (cyclen) (Strem Chemicals); ruthenium(III) chloride (99.98%), 4-aminopyridine (98%), gadolinium(III) chloride hexahydrate (99.999%), potassium bromide (99.99%), human serum albumin (≥ 97%), Hoechst-33342 (≥ 97%), acridine orange (90%), ethidium bromide (~ 95%), propidium iodide (≥ 94%) (Sigma-Aldrich); *tert*-butyl bromoacetate (98%) (Alfa Aesar); 1,10-phenanthroline monohydrate (99.9%), chloroacetyl chloride, potassium carbonate, trifluoroacetic acid (98%), xylenol orange, lithium chloride, sodium acetate (Merck, India) were used as received. HPLC grade water was used for relaxivity studies. Thin layer chromatography was performed on silica gel 60F-254 glass plates. Reaction products were purified by flash chromatography using silica gel (100-200 mesh).

Physical Measurements. Infrared spectra were recorded on a Perkin-Elmer Spectrum RX-I FT IR spectrometer in the range of 4000-400 cm^{-1} using KBr pellets. Electrospray ionization (ESI) mass spectra were recorded on a Quattro-II Triple Quadrupole Mass Spectrometer coupled with waters 2795 HPLC. MALDI-TOF mass spectra were recorded on a Micro Mass TOF Spec 2E Mass Spectrometer using a nitrogen laser (wavelength 337 nm, 4 ns pulse) and α-cyanohydroxy cinnamic acid was used as the matrix. ^1H and ^{13}C NMR spectra were recorded on a Bruker Avance 400 Spectrometer operating at 400 MHz for ^1H and 100 MHz for ^{13}C NMR. Preparative HPLC analyses were carried out using Varian PrepStar 218 (Varian Instruments Inc., USA) binary gradient solvent delivery module equipped with a UV-Vis detector (Model 345) operating in the range 190-1100 nm. Analytical HPLC analyses were performed using 1220 infinity LC system (Agilent Technologies, USA) equipped with a UV-Visible detector operating in the range 190-600 nm (SB-C18 column, 4.6 mm x 250 mm; particle size 5 μm). ICP-OES analyses were performed on a Perkin-Elmer Optima 2000 DV model.

The electronic absorption spectra were recorded on a Shimadzu UV-2450 UV-Vis spectrophotometer, controlled by the UV probe version 2.33 software in the range 190-900 nm at 25 °C using a matched pair of Teflon stoppered quartz cell of path length 1 cm. Fluorescence spectra were recorded on a Fluorolog-3 FL3-221 Spectrofluorometer. The excitation source was a 450 W CW Xenon lamp. The band pass for the excitation and double-grating emission monochromator was set at 2 nm. A matched pair of quartz cell of path length 10 mm was used. All emission spectra were corrected for the instrumental function. All photophysical studies and measurements were made in deoxygenated 0.1 M Tris-HCl buffer (pH = 7.4) using HPLC grade water by purging argon at 25 °C. CHN microanalyses were carried out using Perkin-Elmer 2400 Series II CHNS/O Elemental Analyzer interfaced with the Perkin-Elmer AD6 Autobalance. Helium (99.999% purity) was used as the carrier gas.

Synthesis of the Ligand

1,4,7-Tris(*tert*-butoxymethane)-1,4,7,10 tetraazacyclododecane (*t*-Bu-DO3A) (1). Compound **1** was synthesized by the literature procedure.[39] To a mixture of cyclen (5 g, 29.02 mmol) and sodium bicarbonate (5.80 g, 69.64 mmol) in dry acetonitrile (350 mL) maintained at -5 °C was added *tert*-butyl bromoacetate (13.58 g, 69.64 mmol) dropwise over 30 min under stirring. The reaction mixture was further stirred for 48 h at room temperature, filtered, and flash evaporated to leave a beige solid. The solid product was dissolved in chloroform, filtered to remove the undissolved particles, the filtrate was concentrated, and the resulting solid product was recrystallized from hexane/toluene mixture (2:1, v/v) to afford a white crystalline compound: yield (10.32 g, 69%); m.p. 190 °C. ^1H NMR (400 MHz, $CDCl_3$, 25 °C): δ 3.37 (s, 4 H, $(CH_2)_{2\ acetates}$), 3.29 (s, 2 H, $CH_{2\ unique\ acetate}$), 3.10 (m, 4 H, $(CH_2)_{2\ cyclen\ ring}$), 2.88-2.93 (m, 12 H, $(CH_2)_{2\ cyclen\ ring}$), 1.55 (s, 27 H, $C(CH_3)_{3\ t\text{-}butyl}$); ^{13}C NMR (100 MHz, $CDCl_3$, 25 °C): δ 28.1 (-C-(CH_3)), 47.5 (-$CH_2CH_{2\ cyclic}$

View Article Online
DOI: 10.1039/C5NJ03393D

ring, asymmetric), 49.1 (-CH_2CH_2 cyclic ring, asymmetric), 51.3 (-CH_2CH_2 cyclic ring, symmetric), 58.1 (-CH_2COO^- acetate), 81.6 (-C-$(CH_3)_3$ *t*-butyl), 169.6 (-CH_2COO^- unique acetate), 170.5 (-CH_2COO^- acetate). FT-IR (KBr): 1135 (C-O ester), 1744 (-C=O ester), 2983, 2879 (C-H), 3429 (N-H amine) cm^{-1}. ESI-MS (*m/z*): 515 $[M+H]^+$. Elemental analysis calcd (%) for $[C_{26}H_{51}N_4O_6]$: C, 60.58; H, 9.70; N, 10.87; found: C, 60.34; H, 9.42; N, 10.58.

1,4,7-Tris(carboxymethyl)-1,4,7,10-tetraazacyclododecane (DO3A) (2). A solution of *t*-Bu-DO3A (7 g, 13.58 mmol) in trifluoroacetic acid/dichloromethane (1:1, v/v; 100 mL) was stirred at room temperature for 24 h. The solvent was flash evaporated, the resulting solid product was dissolved in 50 mL methanol, and diethyl ether (250 mL) was added under vigorous stirring. The solid product that precipitated out was filtered, washed with diethyl ether and acetone, and dried in vacuum to get a white crystalline solid: yield (2.58 g, 49%); m.p. 240 °C. FT-IR (KBr): 1724 (C=O acid), 2466 (CH_2 cyclen), 3323 (N-H amine), 3453 (O-H acid) cm^{-1}. ESI-MS (*m/z*): 347 $[M]^+$. Elemental analysis calcd (%) for $[C_{14}H_{26}N_4O_6]$: C, 48.54; H, 7.57; N, 16.17; found: C, 48.26; H, 7.31; N, 15.88.

2-Chloro-*N*-(pyridine-4-yl)acetamide (3). To a solution of 4-aminopyridine (6 g, 63.64 mmol) in dry acetonitrile (300 mL), taken in a double wall RB flask connected to cryogenic circulator water bath, was added potassium carbonate (8.84 g, 63.64 mmol) at -5 °C under stirring over 30 min. A solution of chloroacetyl chloride (7.18 g, 63.64 mmol) in acetonitrile (75 mL) was added slowly to the reaction mixture and stirred for 24 h at room temperature by monitoring the progress of the reaction by TLC (dichloromethane: methanol:aq.NH_3, 9:1:0.1 v/v). The reaction mixture was filtered and flash evaporated to dryness. The resulting crude compound was purified by column chromatography (dichloromethane: methanol:aq.NH_3, 9:1:0.1 v/v) to give a white solid: yield (4.92 g, 38%); m.p. 265 °C (dec). ^{1}H NMR (400 MHz, D_2O, 25 °C): δ 7.89-7.87 (d, 2H, *J* = 8 Hz, CH aromatic), 7.23 (1H, N-H amide), 6.85-6.83 (d, 2H, *J* = 8 Hz, CH aromatic), 3.33 (s, 2H, -CH_2 ethyl); ^{13}C NMR (100 MHz, D_2O, 25 °C): δ 173.2, 158.7, 143.5, 109.6, 60.1. FT-IR (KBr): 1657 (C=O amide), 2992 (CH_2), 3457 (N-H amide) cm^{-1}. ESI-MS (*m/z*): 175 $[M-Cl+K]^+$, 153 $[M-OH]^+$. Elemental analysis calcd (%) for $[C_7H_7N_2ClO]$: C, 49.28; H, 4.14; N, 16.42; found: C, 49.06; H, 4.08; N, 15.97.

1-(*N*-(4-Pyridinyl)acetamido)-1,4,7,10-tetraazacyclododecane-,4,7,10-triacetic acid (DOTA-AMpy) (4). A solution of DO3A (3 g, 8.65 mmol) and potassium carbonate (1.19 g, 8.65 mmol) in water (200 mL) was stirred for 20 min and a solution of 2-chloro-*N*-(pyridine-4-yl)acetamide (1.48 g, 8.65 mmol) in water (50 mL) was added dropwise for 30 min. The reaction mixture was heated at 70 °C for 24 h by monitoring the progress of the reaction by TLC (dichloromethane/methanol/aq.NH_3, 9:1:0.1 v/v), cooled to room temperature, filtered, and flash evaporated to give a white solid. The compound was purified by column chromatography (silica gel, 5% methanol in dichloromethane/aq.NH_3, 9:1 v/v) to give 4 as a white crystalline solid. The purity of the compound was checked by HPLC analysis using acetonitrile/methanol (6:4 v/v) and 0.1% trifluoroacetic acid as the eluent resulting in a single peak (t_R = 3.31 min): yield (2.65 g, 63%); m.p. 290 °C (dec). ^{1}H NMR (400 MHz, D_2O, ppm): δ 7.81-7.79 (d, 2H, *J* = 8 Hz, CH aromatic), 7.20 (1H, N-H amide), 6.77-6.75 (d, 2H, *J* = 8 Hz, CH aromatic), 3.60 (m, 8H, CH_2 acetate), 3.19 (m, 16H, -CH_2 cyclen); ^{13}C NMR (100 MHz, D_2O, ppm): δ 177.6, 173.0, 158.7, 143.4, 109.5, 59.9, 55.3, 49.6. FT-IR (KBr): 1664 (C=O amide), 1716 (C=O acid), 2977 (CH_2), 3437 (O-H acid), 3451 (N-H amide) cm^{-1}. MALDI-MS (*m/z*): 480 $[M]^+$, 524 $[M-2H+2Na]^+$. Elemental analysis calcd (%) for $[C_{21}H_{32}N_6O_7]$: C, 52.49; H, 6.71; N, 17.49; found: C, 52.09; H, 6.45; N, 17.11.

Synthesis of Complexes

[Gd(DOTA-AMpy)(H_2O)] (5). To a solution of **4** (2 g, 4.16 mmol) in water (100 mL) was added $GdCl_3.6H_2O$ (1.54 g, 4.16 mmol) under stirring and the reaction mixture was heated at 65 °C for 8 h by maintaining the pH of the solution at 4.0-6.5 using 0.1 M aqueous HCl. The reaction mixture was cooled to room temperature, filtered, and the filtrate was flash evaporated to yield a hygroscopic solid. Free Gd(III) ions were removed by chelex 100 resin and their absence checked by testing with the arsenazo indicator solution. The gadolinium(III) concentration was determined by ICP-OES: yield (1.72 g, 63%). FT-IR (KBr): 1400 (COO^- acid) 1550 (N-H amide), 1598 (COO^- acid), cm^{-1}. ESI-MS (*m/z*): 633 $[M-H]^+$, 679 $[M-H+2Na]^+$. Elemental analysis calcd (%) for $[C_{21}H_{29}GdN_6O_7]$: C, 38.64; H, 4.79; N, 12.87; found: C, 38.56; H, 4.86; N, 12.98.

[Ru(phen)$_2${Gd(DOTA-AMpy)(H_2O)}$_2$]Cl_2 (7). To a solution of *cis*-[Ru(phen)$_2Cl_2$] (**6**) (0.5 g, 0.93 mmol) in water/ethanol (1:1, v/v) (60 mL) under reflux in an argon atmosphere was added a solution of [Gd(DOTA-AMpy)(H_2O)] (**5**) (1.34 g, 2.05 mmol) in water (25 mL) through a dropping funnel for 15 min and refluxed overnight. The solution was concentrated in a rotavapor and the resulting dark yellow solid was purified by preparative HPLC (acetonitrile: water:TFA, 6:4:0.1 v/v). The fraction was concentrated and dried in vacuum. The purity of the compound was checked by analytical HPLC with acetonitrile/water and 0.1% trifluoroacetic acid as the eluent, resulting in a single peak (t_R = 4.53 min): yield (0.89 mg, 52%). FT-IR (KBr): 1594 (COO^- acid), 1544 (N-H amide), 1412 (COO^- acid) cm^{-1}. UV-Vis λ_{max}(Tris-HCl/nm): 265 (ε/$mol^{-1}dm^3cm^{-1}$ 1,46,166), 473 (18,333). ESI-MS (*m/z*): 556 $[M-2Cl-H_2O+6H]^{3+}$, 615 $[M-H+4Na]^{3+}$. Elemental analysis calcd (%) for $[C_{66}H_{78}N_{16}O_{16}RuGd_2Cl_2]$: C, 44.86; H, 4.45; N, 12.68; found: C, 44.78; H, 4.58; N, 12.79.

[Ru(ttpy){Gd(DOTA-AMpy)(H_2O)}$_3$]Cl_2 (9). To a solution of [Ru(ttpy)Cl_3] (**8**) (0.5 g, 0.94 mmol) in water/ethanol (1:1, v/v) (60 mL) and a few drops of *N*-methyl morpholine under reflux was added a solution of [Gd(DOTA- AMpy)(H_2O)] (**5**) (2.02 g, 3.10 mmol) in water (25 mL) through a dropping funnel for 25 min and refluxed overnight in an argon atmosphere. The solution was concentrated in a rotavapor and the resulting red solid was purified by preparative HPLC (acetonitrile:water:TFA, 6:4:0.1 v/v). The fraction was concentrated and dried in vacuum. The purity of the compound was checked by analytical HPLC with acetonitrile/water and 0.1% trifluoroacetic acid as the eluent, resulting in a single peak (t_R = 5.93 min): yield (0.98 g, 43%). FT-IR (KBr): 1602 (COO^-), 1547 (N-H), 1402 (COO^-) cm^{-1}. UV-Vis λ_{max}(Tris-HCl/nm): 272 (ε/$mol^{-1}dm^3cm^{-1}$ 98,333), 317 (22,166), 493 (4333). ESI-MS (*m/z*): 1209 $[M-2Cl-H_2O+3H+3Na]^{2+}$, 374 $[M-2Cl-5H_2O+H]^{6+}$. Elemental analysis calcd (%) for $[C_{85}H_{110}N_{21}O_{24}RuGd_3Cl_2]$: C, 42.85; H, 4.65; N, 12.34; found: C, 43.01; H, 4.73; N, 12.44.

HPLC analysis and assessment of the purity of the complexes 7 and 9. The purity of the tri- and tetranuclear complexes **7** and **9** were checked by analytical HPLC on a SB-C18 column (Fig. S13 and S15 in the ESI). The complexes were eluted with acetonitrile/ water (6:4,

View Article Online
DOI: 10.1039/C5NJ03393D

v/v) containing 0.1% trifluoroacetic acid. The presence of the complex in the eluate was monitored using the variable wavelength detector. The shorter wavelength of 265 nm for **7** and 273 nm for **9** were chosen due to their high sensitivity toward the impurities. The presence of a single peak suggests that the complexes exist in solution as a single or "averaged" species under the chromatographic conditions employed in this study. The HPLC retention times of complexes **7** and **9** are t_R = 4.53 and 5.93, respectively.

Longitudinal relaxivity measurements. The longitudinal relaxivity of the complexes were determined from the spin-lattice relaxation time (T_1). The T_1 measurements were carried out on a Bruker minispec *mq* 20 NMR Analyzer operating at a frequency of 20 MHz using the standard inversion recovery pulse sequence (180°-τ-90°) with a phase sensitive detection and τ values ranging from 50 μs to 6 s for each concentration of the complex. The temperature was maintained using a temperature console at 37±0.1 °C. The instrument parameters were optimized for each T_1 measurement. Solutions of 0.05, 0.1, 0.15, 0.2, 0.4, 0.6, and 1.2 mM concentration were prepared in phosphate buffer saline (PBS) (pH = 7.4) using HPLC grade water (Merck, India) in 5 mL standard measuring flask (vensil, class "A"). The presence of free gadolinium(III) ion in the solution was checked by xylenol orange test. The T_1 values for each concentration were measured by taking the solution in 180 x 10 mm stoppered glass tube. The computer program "winfit" was used to plot the time versus signal intensity to get a monoexponential plot and T_1 was calculated from the plot. The T_1 curves for all concentrations have a monoexponential decay character. The longitudinal relaxivity was calculated from the slope of the regression line, obtained by the plot of the concentration of the complex versus $1/T_1$, by least square fitting method. The instrument was calibrated by measuring the relaxivity of $[Gd(DO3A)(H_2O)_2]$ in aqueous solution (r_{1p} = 4.80 $mM^{-1}s^{-1}$, 20 MHz, 40 °C).[30]

Preparation of 4.5% (w/v) HSA and GdL/HSA samples. HSA was dissolved in 10 mM sodium phosphate and 150 mM sodium chloride (pH = 7.4) solution. Two HSA solutions (4.5% w/v) were made: one containing the complex with a concentration of 2 mM and the other without the complex.

Ultrafiltration study of binding of Ru-Gd complexes with HSA. Ru^{II}-Gd^{III}/HSA solutions were prepared by combining appropriate amounts of HSA (4.5%, w/v) with solutions of the complexes **7** and **9** of concentrations 0.05, 0.1, 0.15, 0.2, 0.25, 0.4, 0.6, and 1.2 mM. For each study, 1 mL solution was incubated at 37.0±0.1 °C for 20 min, placed in a 30 kDa Ultrafiltration Unit (Amicon), and centrifuged at 3500 g for 10 min. The filtrates were used to measure the concentration of the free Gd(III) complex. Experiments were performed in duplicate. The concentration of gadolinium(III) present in the Ru^{II}-Gd^{III}/HSA solutions and in the ultrafiltrates were determined by ICP-OES.

Cell viability and cytotoxicity study by MTT assay. The HeLa cell lines were grown in a RPMI 1640 medium supplemented with fetal bovine serum (FBS) (10%), penicillin (100 μg mL^{-1}), and streptomycin (100 μg mL^{-1}) and incubated at 37 °C in a humidified incubator with 5% CO_2 and 95% air. Cells at the exponential growth phase were diluted to 2.5 x 10^3 cells/well with RPMI 1640, seeded in 96 well culture clusters (Costar) at a volume of 100 μL per well, and incubated for 24 h at 37 °C. The cells were then treated with different concentrations of the complexes **7** and **9** (5-50 μg mL^{-1}) and incubated for 24 h. A solution of MTT (100 μL, 5 mg mL^{-1}) was added to each well, incubated for a further period of 4 h (37 °C, 5% CO_2), the cell lysate (100 μL) was added to each well, maintained for 12 h at 37 °C, and the plates were analyzed on a Microplate Reader at 570 nm (Biorad 680). The medium and the complex free control samples were prepared simultaneously. The percentage of growth inhibitory rate of the treated cells was calculated using the relationship ($A_{control}$ - $A_{compound}$/$A_{control}$ - $A_{cell\text{-}free}$) x 100 (A is the mean value calculated by using the data from the triplicate tests). The IC_{50} values were determined by plotting the percentage viability versus concentration on a logarithmic graph and reading the concentration at which 50% of cells were viable relative to the control.

Cell viability assay by Hoechst-33342 staining. The HeLa cell lines were seeded into 24 well plates (corning) and grown to approximately 40% confluence. The growth medium was removed and the cells in each well were exposed to 500 μL of the culture medium containing the complexes **7** and **9** (25 and 50 μM) for 24 h. The cells were washed with cold PBS, fixed with 4% paraformaldehyde at room temperature (298 K) for 10 min, washed with cold PBS, labeled with Hoechst-33342 (5 μg mL^{-1} in PBS) for 5 min, and analyzed immediately with a Fluorescence Microscope (Olympus, America).

Morphological assessment of apoptosis by acridine orange (AO) and ethidium bromide (EB) dual staining. The HeLa cell lines were seeded into a 24-well plate (50,000 cells per well) and cultured in a RPMI 1640 medium supplemented with heat inactivated FBS (10%), penicillin (100 μg mL^{-1}), and streptomycin (100 μg mL^{-1}). Cells were maintained at 37 °C in a CO_2 incubator, washed three times with PBS solution, and treated with a PBS solution of the complexes **7** and **9** (25 and 50 μM) and incubated for 24 h at 37 °C. The cells were harvested, washed with PBS, and 40 μL of AO/EB solution (1 part of 100 μg mL^{-1} of AO in PBS; 1 part of 100 μg mL^{-1} of EB in PBS) was added. After staining, the cells were washed with PBS twice, suspended in 200 μL of PBS, and the cell morphology examined under a Fluorescence Microscope (Olympus, America) at 20x resolution.

Flow cytometric analysis of cell cycle by propidium iodide staining. The HeLa cell lines were incubated with the complexes **7** and **9** (25 μM) for 24 h. The cells were harvested and centrifuged (5 min at 800 g), fixed in 2 mL of 70% aqueous ethanol (v/v), incubated for a period of at least 12 h at -20 °C, and centrifuged (15 min at 800 g) and washed twice with ice cold PBS. The cells were resuspended in 200 μL staining solution containing PI (10 μg mL^{-1}) and DNase free RNase (100 μg mL^{-1}) and analyzed by a BD FACSCalibur™ Cytometer (Becton Dickinson, Heidelberg, Germany). The number of cells analyzed for each sample was 10,000 and the experiments were repeated at least three times under identical conditions. Data were collected by BD CellQuest™ Pro software and analyzed by ModFit LT 2.0 software.

Apoptotic DNA ladder assay. The HeLa cell lines were seeded into 24 well plates (triplicate wells of 10^5 cells per well) and incubated with different concentrations of the complexes **7** and **9** in fresh

View Article Online
DOI: 10.1039/C5NJ03393D

DMEM medium for 24 h. The cell samples were collected in 1.5 mL Eppendorf tube, spinned down, resuspended with 0.5 mL PBS in 1.5 mL Eppendorf tubes, and 55 μL of lysis buffer (40 mL of 0.5 M EDTA, 5 mL of 1 M Tris-HCl buffer, pH = 8.0, 5 mL of 100% Triton X-100, and 50 mL water) was added for 20 min on ice (4 °C). The cell samples in the Eppendorf tubes were centrifuged for 30 min, the cells were transferred to new 1.5 mL Eppendorf tubes, the supernatant liquid was extracted with a 1:1 mixture of phenol:chloroform (gentle agitation for 5 min followed by centrifugation), and precipitated in two equivalent of cold ethanol and one-tenth equivalent of sodium acetate. The contents in the Eppendorf tubes were spinned down, decanted, and resuspended the precipitates in 30 μL of deionized water-RNase solution (0.4 mL water and 5 μL RNase) and 5 μL of loading buffer for 30 min at 37 °C. DNA ladder (marker) (2 μL) was inserted on the outer lanes and 1.2% gel was run at 5 V for 5 min before increasing to 100 V. After the dye front reached 75% of the gel, the image of DNA shearing illuminator was monitored at 312 nm using a UV lamp.

Molecular docking study. Molecular docking studies of the complexes **7** and **9** with DNA and HSA were performed using HEX 5.0 software and Q-site finder which is an interactive molecular graphics program for the interaction, docking calculations, and to identify possible binding site of the biomolecules. The coordinates of metal complexes were taken from their optimized structure as a .mol file and were converted to .pdb format using PYMOL software. The crystal structure of B-DNA (PDB ID: 1BNA) and human serum albumin (PDB ID: 1h9z) were retrieved from the protein data bank (http://www.rcsb.org/.pdb). Visualization of the docked systems has been performed using PYMOL Tool. Default parameters were used for the docking calculations with correlation type shape and FFT mode at 3D level, grid dimension of 6 with receptor range 180, ligand range 180 with twist range 360, and distance range 40.

Acknowledgements

We thankfully acknowledge the financial support from the Department of Science and Technology (DST) and the Department of Biotechnology (DBT), Government of India. ESI-MS and MALDI-MS were recorded in SAIF, Punjab University and Jawaharlal Nehru University. The ^{1}H and ^{13}C NMR spectra were recorded in SAIF, IIT-Madras. We thank the Pondicherry Centre for Biological Sciences, Pondicherry, India, for their help in carrying out the cell culture and fluorescence imaging studies.

References

1 *(a)* P. Caravan, J. J. Ellison, T. J. McMurry and R. B. Lauffer, *Chem. Rev*., 1999, **99**, 2293-2352; *(b)* K. W. Y. Chan and W. T. Wong, *Coord. Chem. Rev*., 2007, **251**, 2428-2451; *(c)* A. E. Merbach, L. Helm and E. Toth, *The Chemistry of Contrast Agents in Medical Magnetic Resonance Imaging*; 2nd ed. Wiley, Chichester, U.K. 2013.

2 *(a)* G. M. Edelman, J. R. Hesselink, M. B. Zlatkin and J. V. Crues, *Clinical Magnetic Resonance Imaging*, Elsevier Health, St. Louis, 2006, vol. 3; *(b)* S. Aime, A. Barge, C. Cabella, S. G. Crich and E. Gianolio, *Curr. Pharm. Biotechnol*., 2004, **5**, 509-518.

3 *(a)* P. Caravan, *Chem. Soc. Rev*. 2006, **35**, 512-523; *(b)* E. L. Que and C. J. Chang, *Chem. Soc. Rev*., 2010, **39**, 51-60; *(c)* S. Aime, S. G. Crich, E. Gianolio, G. B. Giovenzana, L. Tei and E. Terreno, *Coord. Chem. Rev*., 2006, **250**, 1562-1579; *(d)* E. Terreno, D. D. Castelli, A. Viale and S. Aime, *Chem. Rev*., 2010, **110**, 3019-3042; (e) K. N. Raymond, V. C. Pierre, *Bioconjugate Chem*., 2005, **16**, 3-8; *(f)* A. J. L. Villaraza, A. Bumb and M. W. Brechbiel, *Chem. Rev*., 2010, **110**, 2921-2959; *(g)* L. M. De Leon-Rodriguez, A. J. M. Lubag, C. R. Malloy, G. V. Martinez, R. J. Gillies and A. D. Sherry, *Acc. Chem. Res*., 2009, **42**, 948-957.

4 A. Beeby, S. W. Botchway, I. M. Clarkson, S. Faulkner, A. W. Parker, D. Parker and A. G. Williams, *J. Photochem. Photobiol. B* 2000, **57**, 83-89.

5 L. E. Jennings and N. J. Long, *Chem. Commun*., 2009, 3511-3524.

6 *(a)* A. Louie, *Chem. Rev*., 2010, **110**, 3146-3195; *(b)* C. S. Bonnet and E. Toth, *C. R. Chim*., 2010, **13**, 700-714; *(c)* L. Frullano and T. J. Meade, *J. Biol. Inorg. Chem*., 2007, **12**, 939-949.

7 *(a)* E. Debroye and T. N. Parac-Vogt, *Chem. Soc. Rev*., 2014, **43**, 8178-8192; *(b)* P. Verwilst, S. Park, B. Yoon and S. Kim, *Chem. Soc. Rev*., 2015, **44**, 1791-1806.

8 *(a)* S. Faulkner, B. P. Burton-Pye and S. J. A. Pope, *Appl. Spectrosc. Rev*., 2005, **40**, 1-39; *(b)* J.-C. G. Bunzli and C. Piguet, *Chem. Soc. Rev*., 2005, **34**, 1048-1077; *(c)* V. Fernandez-Moreira, F. L. Thorp-Greenwood and M. P. Coogan, *Chem. Commun*., 2010, **46**, 186-202; *(d)* E. Baggaley, J. A. Weinstein and J. A. G. Williams, *Coord. Chem. Rev*., 2012, **256**, 1762-1785; *(e)* D.-L. Ma, H.-Z. He, D. S.-H. Chan and C.-H. Leung, *Angew. Chem. Int. Ed*., 2013, **52**, 7666-7682; *(f)* K. K.-W. Lo and K. Y. Zhang, *RSC Adv*., 2012, **2**, 12069-12083; *(g)* K. K.-W. Lo, M.-W. Louie and K. Y. Zhang, *Coord. Chem. Rev*., 2010, **254**, 2603-2622; *(h)* K. K.-W. Lo, S. P.-Y. Li and K. Y. Zhang, *New. J. Chem*., 2011, **35**, 265-289; *(i)* K.K.-W. Lo, K. Y. Zhang and S. P.-Y. Li, *Pure Appl. Chem*., 2011, **83**, 823-840; *(j)* K. K.-W. Lo, M.-W. Louie, K. Y. Zhang and S. P.-Y. Li, *Eur.J. Inorg. Chem*., 2011, 3551-3568; *(k)* J.-C. Bunzli, *Chem. Rev*., 2010, **110**, 2729-2755; *(l)* E. J. New, D. Parker, D. G. Smith and J. W. Walton, *Curr. Opin. Chem. Biol*., 2010, **14**, 238-246; *(m)* M. P. Coogan and V. Fernandez-Moreira, *Chem. Commun*., 2014, **50**, 384-399.

9 *(a)* V. Comblin, D. Gilsoul, M. Hermann, V. Humblet, V. Jacques, M. Mesbahi, C. Sauvage and J. F. Desreux, *Coord. Chem. Rev*., 1999, **185**, 451-470; *(b)* J. B. Livramento, E. Toth, A. Sour, A. Borel, A. E. Merbach and R. Ruloff, *Angew. Chem. Int. Ed*., 2005, **44**, 1480-1484; *(c)* J. Costa, R. Ruloff, L. Burai, L. Helm and A. E. Merbach, *J. Am. Chem. Soc*., 2005, **127**, 5147-5157; *(d)* J. B. Livramento, A. Sour, A. Borel, A. E. Merbach and E. Tóth, *Chem.-Eur. J*., 2006, **12**, 989-1003; *(e)* T. N. Parac-Vogt, L. Vander Elst, K. Kimpe, S. Laurent, C. Burtea, F. Chen, R. Van Deun, Y. C. Ni, R. N. Muller and K. Binnemans, *Contrast Media Mol. Imaging* 2006, **1**, 267-278; *(f)* J. Paris, C. Gameiro, V. Humblet, P. K. Mohapatra, V. Jacques and J. F. Desreux, *Inorg. Chem*., 2006, **45**, 5092-5102.

10 *(a)* T. Koullourou, L. S. Natrajan, H. Bhavsar, J. A. Simon, J. H. Feng, J. Narvainen, R. Shaw, E. Scales, R. Kauppinen, A. M. Kenwright and S. Faulkner, *J. Am. Chem. Soc*., 2008, **130**, 2178-2179; *(b)* G. Dehaen, S. V. Eliseeva, K. Kimpe, S. Laurent, L. Vander Elst, R. N. Muller, W. Dehaen, K. Binnemans and T. N. Parac-Vogt, *Chem.-Eur. J*., 2012, **18**, 293-302; *(c)* E. Debroye, G. Dehaen, S. V. Eliseeva, S. Laurent, L. Vander Elst, R. N. Muller, K. Binnemans and T. N. Parac-Vogt, *Dalton Trans*., 2012, **41**, 10549-10566.

11 Q. Zhao, C. Huang and F. Li, *Chem. Soc. Rev*., 2011, **40**, 2508-2524.

12 L. Moriggi, A. Aebischer, C. Cannizzo, A. Sour, A. Borel, J.-C. G. Bünzli and L. Helm, *Dalton Trans*., 2009, 2088-2095.

13 G. Dehaen, P. Verwilst, S. V. Eliseeva, S. Laurent, L. Vander Elst, R. N. Muller, W. M. De Borggraeve, K. Binnemans and T. N. Parac-Vogt, *Inorg. Chem*., 2011, **50**, 10005-10014.

View Article Online
DOI: 10.1039/C5NJ03393D

14 G. Dehaen, S. V. Eliseeva, P. Verwilst, S. Laurent, L. Vander Elst, R. N. Muller, W. D. Borggraeve, K. Binnemans and T. N. Parac-Vogt, *Inorg. Chem*., 2012, **51**, 8775-8783.
15 A. Boulay, C. Deraeve, L. Vander Elst, N. Leygue, O. Maury, S. Laurent, R. N. Muller, B. Mestre-Voegtle and C. Picard, *Inorg. Chem*., 2015, **54**, 1414-1425.
16 P. Verwilst, S. V. Eliseeva, L. Vander Elst, C. Burtea, S. Laurent, S. Petoud, R. N. Muller, T. N. Parac-Vogt and W. M. De Borggraeve, *Inorg. Chem*., 2012, **51**, 6405-6411.
17 I. Mamedov, T. N. Parac-Vogt, N. K. Logothetis and G. Angelovski, *Dalton Trans*., 2010, **39**, 5721-5727.
18 E. Debroye, M. Ceulemans, L. Vander Elst, S. Laurent, R. N. Muller and T. N. Parac-Vogt, *Inorg. Chem*., 2014, **53**, 1257-1259.
19 *(a)* M. R. Gill and J. A. Thomas, *Chem. Soc. Rev*., 2012, **41**, 3179-3192; *(b)* H. Ke, H. Wang, W.-K. Wong, N.-K. Mak, D. W. Kwong, K.-L. Wong and H.-L. Tam, *Chem. Commun*., 2010, **46**, 6678-6680; *(c)* M. J. Pisani, P. D. Fromm, Y. Mulyana, R. J. Clarke, H. Körner, K. Heimann, J. G. Collins and F. R. Keene, *ChemMedChem*., 2011, **6**, 848-858.
20 M. R. Gill, J. Garcia-Lara, S. J. Foster, C. Smythe, G. Battaglia and J. A. Thomas, *Nat. Chem*., 2009, **1**, 662-667.
21 K. E. Erkkila, D. T. Odom and J. K. Barton, *Chem. Rev*., 1999, **99**, 2777-2796.
22 C. A. Puckett, R. J. Ernst and J. K. Barton, *Dalton Trans*., 2010, **39**, 1159-1170.
23 N. P. Cook, V. Torres, D. Jain and A. A. Marti, *J. Am. Chem. Soc*., 2011, **133**, 11121-11123.
24 A. Nithyakumar and V. Alexander, *Dalton Trans*., 2015, **44**, 17800-17809.
25 *(a)* W. Spahni and G. Calzaferri, *Helv. Chim. Acta*., 1984, **67**, 450-454; *(b)* F. H. Case and T. J. Kasper, *J. Am. Chem. Soc*., 1956, **78**, 5842-5844.
26 B. P. Sullivan, D. J. Salmon and T. J. Meyer, *Inorg. Chem*., 1978, **17**, 3334-3341.
27 P. A. Adcock, F. R. Keene, R. S. Smythe and M. R. Snow, *Inorg. Chem*., 1984, **23**, 2336-2343.
28 L. J. Carbonniere, S. Faulkner, C. Platas-Iglesias, M. Regueiro-Figueroa, A. Nonat, T. Rodriguez-Blas, A. De-Blas, W. S. Perry and M. Tropiano, *Dalton Trans*., 2013, **42**, 3667-3681.
29 J. P. Andre, E. Toth, H. Fischer, A. Seelig, H. R. Macke and A. E. Merbach, *Chem.-Eur. J*., 1999, **10**, 2977-2982.
30 S. I. Kang, R. S. Ranganathan, J. E. Emswiler, K. Kumar, J. Z. Gougoutas, M. F. Malley and M. F. Tweedle, *Inorg. Chem*., 1993, **32**, 2912-2918.
31 J. E. Jones, A. J. Amoroso, I. M. Dorin, G. Parigi, B. D. Ward, N. J. Buurma and S. J. A. Pope, *Chem. Commun*., 2011, **47**, 3374-3376.
32 T. Mosmann, *J. Immunological Mds*., 1983, **65**, 55-63.
33 J. van Meerloo, G. J. L. Kaspers and J. Cloos, "Cell Sensitivity Assays: The MTT Assay"; *In Cancer Cell Culture: Methods and Protocols*; 2nd ed.; I. A. Cree, Ed.; Methods in Molecular Biology; Springer Science, 2011, Vol. 731, Chapter 9, pp 237-246..
34 *(a)* S. A. Latt, G. Stetten, L. A. Juergens, H. F. Willard and C. D. Scher, *J. Histochem. Cytochem*., 1975, **23**, 493-505; *(b)* S. A. Latt and G. Stetten, *J. Histochem. Cytochem*., 1976, **24**, 24-33.
35 A. J. McGahon, S. J. Martin, R. P. Bissonnette, A. Mahboubi, Y. Shi, R. J. Mogil, W. K. Nishioka and D. R. Green, *Methods in Cell Biology*; Eds. L. M. Schwartz and B. A. Osborne, Academic Press, New York, 1995, Vol. 46, Chapter 9, pp 153-185.
36 *(a)* A. J. Krishan, *Cell Bio*., 1975, **66**, 188-193; *(b)* C. Riccardi and I. Nicoletti, *Nature Protoc*., 2006, **1**, 1458-1461.
37 A. H. Wyllie, *Nature* 1980, **284**, 555-556.
38 *(a)* N. C. Seeman, H. Wang, X. Yang, F. Liu, C. Mao, W. Sun, L. Wenzler, Z. Shen, R. Sha, H. Yan, M. H. Wong, P. Sa-Ardyen, B. Liu, H. Qiu, X. Li, J. Qi, S. M. Du, Y. Zhang, J. E. Mueller, T.-J. Fu, Y. Wang and J. Chen, *Nanotechnology* 1998, **9**, 257-273; *(b)* S. Arnott, *Nature* 1986, **320**, 313.
39 S. Mizukami, K. Tonai, M. Kaneko and K. Kikuchi, *J. Am. Chem. Soc*., 2008, **130**, 14376-14377.

View Article Online
DOI: 10.1039/C5NJ03393D

Table of contents

A tri- (Ru^{II}-Gd_2^{III}) and tetranuclear (Ru^{II}-Gd_3^{III}) *d-f* heterometallic complexes which function as contrast agents for MRI and as optical probes for fluorescence imaging are reported. In vitro studies with the HeLa cell lines show that the complexes exhibit anticancer activity.